WAVEFRONT TOMOGRAPHY WITH DIFFRACTION-ONLY 3D P-CABLE DATA

M. Glöckner, D. Gajewski, S. Muff, and C. Berndt

email: *martina.gloeckner@uni-hamburg.de*

keywords: *p-cable,diffractions,velocity model*

ABSTRACT

P-cable data often do not allow model building by conventional methods because of an insufficient offset to target ratio. Diffractions, however, provide a tool for model building, even for Zero-Offset data. Here, we introduce a diffraction-based velocity analysis that provides seismic velocity information without the need of acquiring ocean bottom seismometer data. The diffraction based processing uses a multiparameter stacking operator which naturally enhances diffractions and at the same time generate kinematic wavefield attributes. These attributes together with the stack serve as input for a wavefront tomography and generate a depth velocity model in an automated fashion. An additional advantage of diffraction tomography is the scatter potential which yields a large area of illumination in the tomography compared to a pure reflection processing. The illuminated area is two to three times larger and more velocity information can be calculated from the same amount of data.

INTRODUCTION

During a cruise with the german research vessel Sonne in 2016 (Berndt et al., 2016) we investigated the 1888 flank collapse of volcanic island called Ritter Island which is located about 100 km (62 miles) northeast of New Guinea. Ritter Island is part of the 1000 km (621 miles) long Bismarck volcanic arc. It is surrounded by steep volcanic islands and marine sediment transport is unknown but supposed to be dominated by erosion from landslides and pyroclastic flows. The flank collapse is the largest historic flank collapse of a volcanic island and generated a tsunami well-documented by german colonists.

Because of very dense sampling at near offsets 3D seismic data acquired with P-cable systems provide very high resolution of 3x3x3 m. However, because of very short (12.5-100 m long) streamers their processing has so far been dependent on a priori information from long-offset 2D seismic surveys or ocean bottom seismometers that were deployed during or after the P-cable acquisition. Here, we reanalyse a data set that was recorded in the Bismarck volcanic arc, Papua New Guinea in 2016. The overall aim of this study is to investigate the flank collapse of a volcano and estimate the tsunami potential for similar cases (Berndt et al., 2016). The P-cable data are used to reveal the distribution and configuration of the flank material that has slid down from the volcano. However, so far the data were only migrated using a constant velocity (1500 m/s), because the data do not allow the derivation of velocity fields due to the short streamers.

Diffractions have the potential to fill this gap (Bauer et al., 2017). Khaidukov et al. (2004) show the potential of a diffraction-based data processing, e.g. small-scale structures are enhanced in resolution. Diffractions have to be carefully and accurately separated from reflections. Different separation techniques are used, e.g. stacking along diffraction traveltime curves (for example Dell and Gajewski, 2011), decomposition of diffracted and reflected wavefield (see Taner et al., 2006) or using a modified Kirchhoff migration (see Kozlov et al., 2004). Multiparameter stacking techniques provide the benefit from having

kinematic wavefield attributes (Hubral, 1983). These can be further used to calculate a depth velocity model by performing a wavefront tomography (Duveneck, 2004).

THEORY

To obtain a final depth velocity model we start with a multiparameter stack. Walda et al. (2017) show that different multiparamter stacking operator, e.g. common-reflection-surface (CRS) stack (Bergler et al., 2002), Multifocusing (Landa et al., 2010) or non-hyperbolic CRS (Fomel and Kazinnik, 2013), perform similar in speed and accuracy. Therefore, we decide to use the non-hyperbolic CRS because it is most suitable for diffraction processing. Equation 1 shows the operator:

$$t = \sqrt{\Big[\frac{1}{4}\sqrt{F(t_0, \vec{m} - \vec{h})} \cdot \sqrt{F(t_0, \vec{m} + \vec{h})}\Big]^2 + 2t_0 \vec{h}^{\mathbf{T}} \big(\mathbf{M} - \mathbf{N}\big)\vec{h}}, \tag{1}$$

where $\vec{m}$ is the midpoint in x and y direction and $\vec{h}$ is the offset vector, respectively, t_0 is the zero-offset traveltime and F denotes

$$F(t_0, \vec{m}) = \big(t_0 + 2\vec{p}^{\mathbf{T}}\vec{m}\big)^2 + 2t_0 \vec{m}^{\mathbf{T}}\mathbf{N}\vec{m}. \tag{2}$$

The parameters can be transformed in the well-known kinemactic wavefield attributes:

$$\vec{p} = \frac{\sin\alpha}{v_0}\Big(\cos\beta \sin\beta\Big), \mathbf{M} = \frac{1}{v_0}\mathbf{R}\mathbf{K}_{\mathrm{NIP}}\mathbf{R}^{\mathbf{T}}, \mathbf{N} = \frac{1}{v_0}\mathbf{R}\mathbf{K}_{\mathrm{N}}\mathbf{R}^{\mathbf{T}}, \tag{3}$$

where $\mathbf{R}$ is a rotation matrix towards a ray-centered coordinate system and $\mathbf{K}_{\mathrm{N}}$ and $\mathbf{K}_{\mathrm{NIP}}$ are the curvature matrices representing the normal (N) wave and the normal-incident point (NIP) wave. The angle α and β represent dip and azimuth angle. Attributes can be calculated without the offset information for diffractions with the assumption of point scatterers. Point diffractors represent tip diffractors in the geological interpretaion and contain same information in midpoint direction, too. The stacked data can be used for a diffraction separation. This is done by a dip filter due to the early stage of the work progress. Afterwards the separated data are stacked again to obtain the kinematic wavefield attributes for the diffracted wavefield. These are: the dip and azimuth angle as well as two curvature matrices. In the diffraction case NIP wave and N wave are similar. Bauer et al. (2017) show that it is possible to use only diffracted data as input for wavefront tomography and obtain a reliable velocity model suitable for depth migration. The wavefront tomography uses the kinematic wavefield attributes. Curvatures are focused at zero time to obtain the velocity model in depth.

APPLICATION

The 3D data set was acquired with the GEOMAR P-cable system consisting of 16 digital streamers manufactured by Geometrics. Four are solid state and 12 oil filled. Each has eight hydrophone groups. The offsets between gun and receivers varied between 160 and 320 m. We used 2 GI guns with 105/105 cubic inch in harmonic mode at a pressure of 3000 psi. Towing speed was between 3 and 3.5 knots and shot interval approximately 10 m. Source and receiver positions were determined from three GPS antennas and refined by calculating direct wave arrival times.

Figure 1 shows the original data. The uppermost event represents the volcanic cone. Further events are visible in the deeper parts of the flanks of the cone.

Figure 2 shows the separated and stacked diffractions of the same inline. In comparison with the original data (Figure 1) the signal-to-noise ratio is improved. The volcanic cone (uppermost event) is disrupted due to the dipfiltering. Nevertheless, other diffractions are visible and horizontal events disappeared.

Figure 3 shows the focused endpoints and a slice of the velocity within the model. The water column is set constant and the seafloor starts between 700 to 800 m. Velocities increase with a maximum in the middle representing the volcanic cone. It is not visible on the seafloor due to vertical exaggeration. Please note, that the endpoints are spread over a large area, which means a good ray coverage and illumination for the

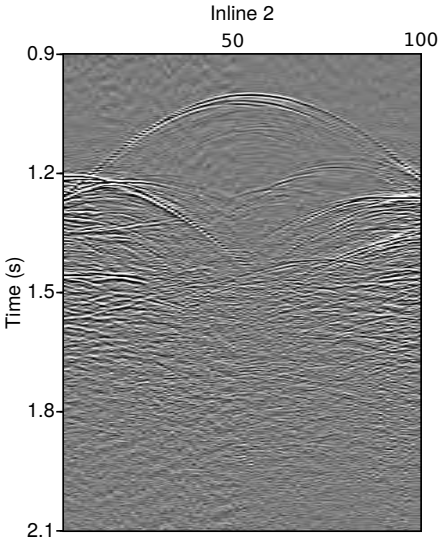

Figure 1: Original data.

tomography.
Figure 4 shows the benefits of a diffraction processing in 3D with wavefront tomography. The selected data, from which the attributes are calculated, are shown in the blue box. For the tomography, we are able to choose a larger area for velocity determination due to the performed diffraction processing. Nevertheless, there is even more room for calculations because ray endpoints are also given outside the green box. Diffractions yield due to their physical behaviour (scatterer) an increased resolution. If we would consider only reflections, velocity informations are only available in the blue box.

CONCLUSIONS

We introduce a processing workflow based on diffractions for a 3D P-cable data set. Multiparameter stacking and dipfiltering lead to diffraction-only data. They are used for a wavefront tomography and the depth velocity model is calculated. The advantage of diffractions is the large illumination of the tomography model which can never be achieved with a pure reflection processing. The scattered energy of diffractions spreads over a large area and velocities can be reliable determined due to good ray coverage. The early stage of the work leaves room for improvements. We will perform an advanced diffraction separation using coherence subtraction (Schwarz and Gajewski, 2017) to improve the results of the wavefront tomography. A suitable depth velocity model will allow us to perform a reverse-time migration and obtain a final image in depth with a high resolution.

ACKNOWLEDGEMENTS

We thank the members of the Applied Seismics Group Hamburg, especially Jan Walda for continious help in improving performance of the 3D processing and Sergius Dell for discussions. This work was kindly supported by the sponsors of the Wave Inversion Technology (WIT) Consortium.

REFERENCES

Bauer, A., Schwarz, B., and Gajewski, D. (âĂć2017). Utilizing diffarctions in wavefront tomography. *Geophysics*, 82(2).

Bergler, S., Hubral, P., Marchetti, P., Cristini, A., and Cardonne, G. (2002). 3d common-reflection-surface stack and kinematic wavefield attributes. *The Leading Edge*, 21(10).

Berndt, C., Muff, S., Klaucke, I., Watt, S., Böttner, C., Schramm, B., Völsch, A.-M., Bennecke, S., Elger,

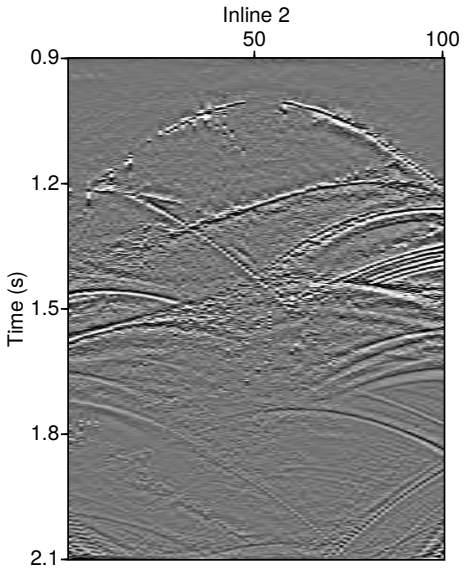

Figure 2: Final diffraction stack.

J., Chi, W.-C., Van Haren, J., Micallef, A., and Roth, T. (2016). RV SONNE 252 Cruise Report / Fahrtbericht Tsunami potential of volcanic flank collapses Table of content. Technical report.

Dell, S. and Gajewski, D. (2011). Common-reflection-surface-based workflow for diffraction imaging. *Geophysics*, 76.

Duveneck, E. (2004). Velocity model estimation with data-derived wavefront attributes. *Geophysics*, 69:265–274.

Fomel, S. and Kazinnik, R. (2013). Non-hyperbolic common reflection surface stack. *Geophysical Prospecting*, 61:21–27.

Hubral, P. (1983). Computing true amplitude reflections in a laterally inhomogeneous earth. *Geophysics*, 48:1051–1062.

Khaidukov, V., Landa, E., and Moser, T. J. (2004). Diffraction imaging by focusing-defocusing: An outlook on seismic superresolution. *Geophysics*, 69(10):1478–1490.

Kozlov, E., Barasky, N., Korolev, E., Geophysical Alexander Antonenko, P., and Koshchuk, E. (2004). Imaging scattering objects masked by specular reflections. *74th Ann. Internat. Mtg. Soc. Expl. Geophys.*

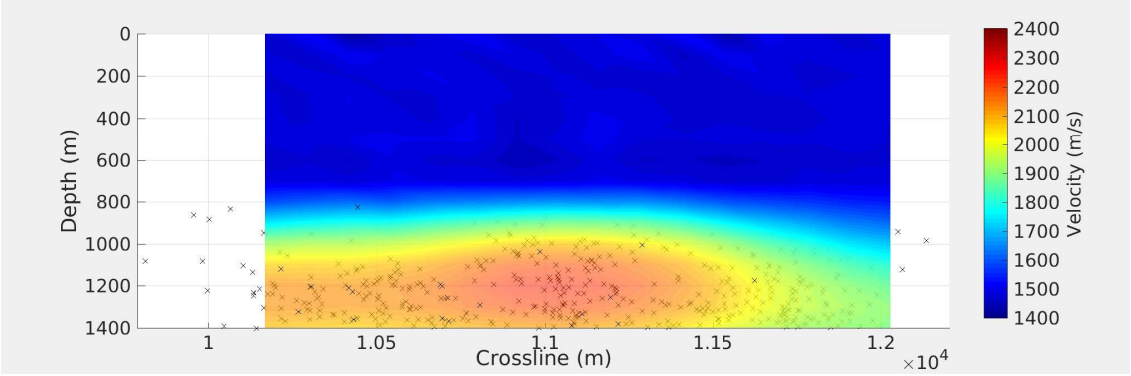

Figure 3: Calculated endpoints and final velocity model after wavefront tomography.

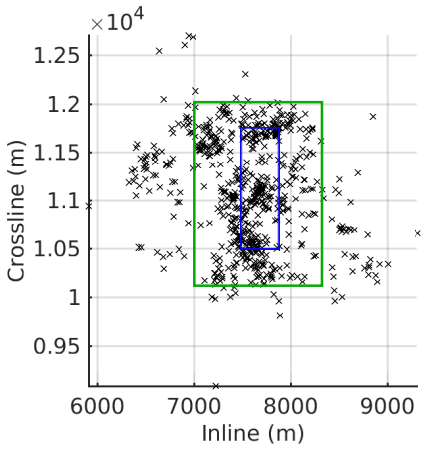

Figure 4: Original data volume (blue), area for wavefront tomography (green), where velocity is calculated and ray endpoints of tomography (x).

Landa, E., Keydar, S., and Moser, T. J. (2010). Multifocusing revisited - inhomogenious media and curved interfaces. *Geophysical Prospecting*.

Schwarz, B. and Gajewski, D. (2017). Accesing the diffracted wavefield by coherent subtraction. *Geophysical Journal International*, 211:45–49.

Taner, M., Fomel, S., and Landa, E. (2006). Separation and Imaging of Seismic Diffractions Using Plane-wave Decomposition. *76th Ann. Internat. Mtg. Soc. Expl. Geophys.*

Walda, J., Schwarz, B., and Gajewski, D. (2017). A competitive comparison of multiparameter stacking operators. *Geophysics*, 82(4):V275–V283.